ChemComm



COMMUNICATION

View Article Online



Cite this: DOI: 10.1039/d5cc04864h

Received 23rd August 2025, Accepted 27th October 2025

DOI: 10.1039/d5cc04864h

rsc.li/chemcomm



Mingyuan Zhang,^a Linxia Cui,^a Yang Jiang,^a Rui Gao,^a Haigang Hao*^a and Meilan Huang (1) *

The direct synthesis of acetic acid from natural gases has attracted great attention. However, achieving selective C–C coupling remains a major challenge. We designed doped single-atom transition metal catalysts on 2D materials, guided by DFT calculations on the reaction pathways for acetic acid synthesis *via* CH₄/CO₂ coupling. Among the catalysts examined, Ni–Si@h-BN shows strong electron synergy in CH₄ activation and C–C coupling under the E–R mechanism, confirmed by kinetics

Transforming CH₄ and CO₂ into acetic acid offers a green route to convert greenhouse gases into value-added chemicals.1 Understanding the reaction mechanism is essential for catalyst design: CH₄ first dissociates into CH₃* and H*, after which CH₃* couples with CO₂ to form CH₃COO*. This intermediate undergoes hydrogenation to yield CH3COOH, which subsequently desorbs as acetic acid.² Homogeneous catalysts like Pd(OAc)₂/Cu(OAc)₂/K₂S₂O₈/CF₃COOH,³ RhCl₃⁴ and PdSO₄⁵ have been used for this conversion, but it is challenging to recycle the catalysts. More practical heterogeneous catalysts use supports like TiO₂, Al₂O₃, SiO₂ and zeolites, with active sites such as Zn or Cu.⁶ For instance, Cu-K-ZSM-5 zeolite⁷ converts CH₄ and CO₂ to acetic acid at 500 °C, achieving 5% CH₄ conversion and 100% acetic acid selectivity after 1 hour, while ZnO-CeO2 supported on montmorillonite⁸ achieves 8.33% CH₄ conversion and 100% selectivity at 300 °C. Zn-based catalysts generally show higher activity than Cu-based ones but they still require stringent conditions for effective activation. Theoretical calculations can underpin experimental efforts to improve catalyst activity by revealing reaction pathways and energy barriers. In particular, understanding the elementary steps of C-H activation and subsequent C-C coupling is especially important for the direct synthesis of acetic acid catalysts.10 Langmuir-Hinshelwood (L-H) and

Eley-Rideal (E-R) mechanisms are two commonly adopted mechanisms for CO2-CH3* coupling. Nie et al.11 found that Fe/ZnO2 catalysts activate CH4 efficiently due to Fe-Zn bimetallic synergy, with low barriers for CH₄ activation (0.30 eV) and C-C bond formation (0.75 eV) via the L-H pathway. However, the L-H mechanism requires dual adsorption sites, which increases the probability of side reactions. 12 The E-R mechanism, involving reactions between gas-phase molecules and adsorbed species, usually reflects experimental conditions. 13 When CH₄ and CO₂ compete for adsorption sites, the relative adsorption strengths govern which pathway becomes dominant. In the Zn-ZSM-5 catalysts, 14 CH₄ preferentially adsorbs on Zn2+ sites to form CH3* intermediates, while CO2 shows weak affinity (<0.2 eV), and thus gas-phase CO2 couples directly with adsorbed CH3 following an E-R mechanism. Although Zn-ZSM-5 lowers the barriers for CH₄ activation (0.65 eV) and acetate formation (0.20 eV), its C-C coupling activity remains limited (1.79 eV), underscoring the need to exploit selective C-C bond formation by other transition metal catalysts under the E-R pathway. Catalysts with well-defined single-site active units¹⁵—such as isolated metal atoms with specific coordination environments or tailored metal-support interfaces—are highly promising for enhancing C-C coupling via the E-R mechanism.

Nickel is commonly used for CH₄ conversion due to its high activity, but it is prone to coking and sintering. ¹⁶ Studies show that adding Si atoms in Ni–Si/ZrO₂ catalysts enhances Ni dispersion, stability, and resistance to coking during CH₄ and CO₂ dry reforming. ¹⁷ This inspired us to examine the effect of Si on the electron density of Ni-based catalysts, to optimize Ni sites for coupling CH₄ and CO₂ into acetic acid. On the other hand, single-atom catalysts (SACs) on 2D materials have shown significant potential for CO₂ conversion, owing to their high atom utilization and activity, for example, Feng *et al.* demonstrated that SACs embedded in a 2D graphitic carbon nitride support exhibit high catalytic efficiency. ¹⁸ For example, Zn-based metal oxide SACs show unique catalytic properties for

^a School of Chemistry and Chemical Engineering, Inner Mongolia University, Hohhot, Inner Mongolia 010021, China. E-mail: haohaigang@imu.edu.cn

^b School of Chemistry and Chemical Engineering, Queen's University, Belfast, BT9 5AG, UK. E-mail: m.huang@qub.ac.uk

This article is licensed under a Creative Commons Attribution 3.0 Unported Licence.

Open Access Article. Published on 28 2025. Downloaded on 07-11-2025 9:04:01.

Communication

ChemComm

converting CH₄ and CO₂ to acetic acid; however, efficient C-C coupling remains a challenge. 19 The high surface area and stability of two-dimensional (2D) materials enable SACs@2D systems with well-defined active centres, surpassing conventional metal oxide supports²⁰ and potentially improving C-C coupling. Herein, we designed SACs composed of transition metals (Mn, Fe, Co, and Ni) doped with Si promoters on h-BN (TM-Si@h-BN) to identify the optimal active component. Subsequently, we evaluated various 2D materials, including graphene (GR), N₄-doped graphene (N₄@GR), and phosphorene (P), to determine the optimal catalyst configuration. We demonstrated that Ni-Si@h-BN is a promising alternative to traditional catalysts and elucidated its activation and reaction mechanism: electron transfer from Si to Ni creates an electronrich Ni site (Ni^{-2.16}) and its moderate work function is favourable for electron balance, facilitating CH₄ activation and CO₂ adsorption.

The computed binding energy (E_b) and formation energy $(E_{\rm f})^{21}$ for TM-Si@h-BN catalysts demonstrate the stability of Si and TM atoms on h-BN (Table S1). AIMD simulations of the TM-Si@h-BN catalyst structure at 500 K demonstrate its thermodynamic stability (Fig. S1a and b). Bader charge calculations (Table S1) show electron transfer from Si to transition metals, forming a $TM_1^{\delta^-} - Si_1^{\delta^+}$ distribution. We compared the adsorption abilities of CH4 and CO2 at 500 K. Although both CH4 and CO2 exhibit relatively weak interactions with the surfaces, CH4 binds more strongly (-0.36 to 0.15 eV) than CO_2 (0.22-0.65 eV) on all TM-Si@h-BN catalysts, underscoring that CH4 is preferentially activated across these materials (Fig. S1c and d). The work function (Fig. S2), reflecting the electron transfer ability of TM-Si@h-BN, controls CH₄ and CO₂ adsorption such that CH₄

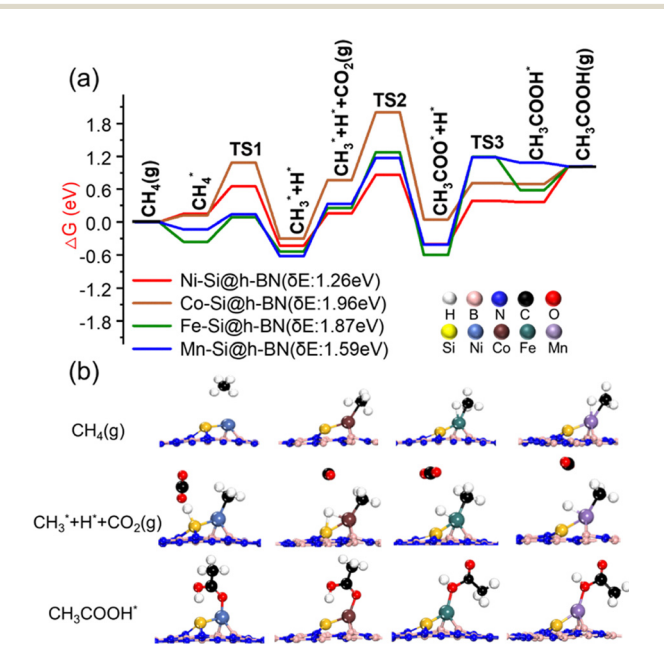


Fig. 1 The coupling of CH₄ and CO₂ into acetic acid on TM-Si@h-BN at 500 K. (a) Reaction energy profile (energy span, δE is shown in parentheses). (b) Adsorption configurations of key reactants and products. See Fig. S6 and Table S4 for details

adsorption weakens with increasing work function, while CO₂ adsorption strengthens (Fig. S3a).

The dissociation of CH3* at TM sites is influenced by the presence of doped Si. On Mn-Si@h-BN and Fe-Si@h-BN, the H atom is co-adsorbed with CH₃* on the top site of TM, exhibiting low energy barriers of 0.27 and 0.44 eV (Fig. 1 and Table S4), respectively. On Co-Si@h-BN, H* prefers the Co-Si bridge site, with a higher barrier of 0.96 eV. On Ni-Si@h-BN, the hydrogen atom migrates to the top site of Si, incurring an energy barrier of 0.50 eV. The C-C coupling is initiated by the reaction of CH₃* and gaseous CO2, forming the CH3COO* intermediate at TM sites via the E-R mechanism. Ni-Si@h-BN shows the lowest barrier for this step (0.71 eV) among the TM-Si@h-BN catalysts, and crystal Hamilton population (COHP) analysis reveals a weaker Ni-CH₃ bond (integrated strength ICOHP: -1.18 eV) that facilitates CO₂ insertion (Fig. S7). The hydrogenation of CH₃COO* to acetic acid generally proceeds with high barriers on TM-Si@h-BN. Furthermore, the energetic span model (δE) was employed as a direct descriptor of the catalytic cycle rate.²² At 500 K, except for Mn-Si, where TS3 (CH₃COO* hydrogenation) is the turnover-determining transition state (TDTS), TS2 (C-C coupling) serves as the TDTS for the other TM-Si systems, while CH3COO* + H* acts as the turnover-determining intermediate (TDI) in all cases. The corresponding δE values for each system are summarized in Table S12. Notably, Ni-Si@h-BN shows the lowest δE (1.26 eV), emphasizing its superior activity and highlighting its potential as a 2D support for further optimization.

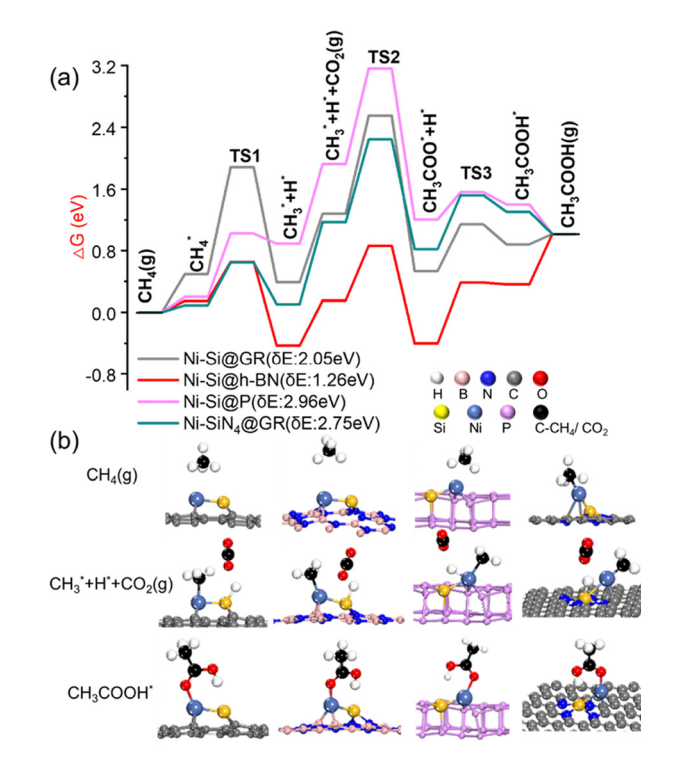


Fig. 2 The coupling of CH₄ and CO₂ into acetic acid on Ni-Si@2D at 500 K. (a) Reaction energy profile (energy span, δE is shown in parentheses). (b) Adsorption configurations of key reactants and products. See Fig. S9 and Table S9 for details

ChemComm Communication

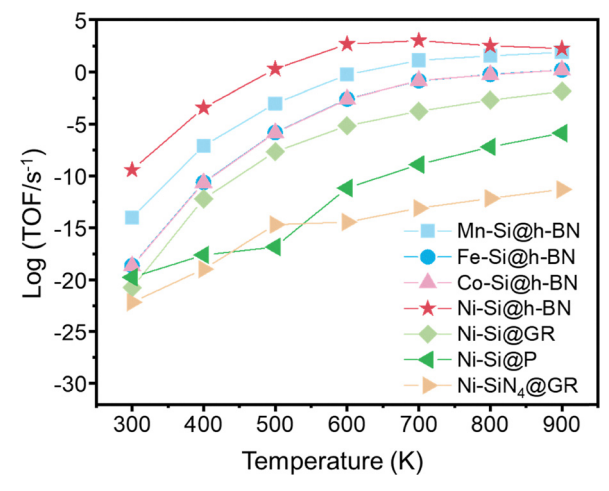


Fig. 3 Turnover frequencies for CH₃COOH production over TM-Si@2D as a function of temperature (CH₄/CO₂ = 1:1, 1 bar).

The structural stability of Ni-Si@2D and the thermodynamic stability of Ni-Si@2D at 500 K are confirmed (Fig. S8). Bader charge analysis reveals that silicon donates electrons to transition metals on both Ni-Si@2D and TM-Si@h-BN catalysts, highlighting its general role as an electron donor (Table S5), and accounting for the stronger CH₄ adsorption observed on TM-Si@2D compared to TM@2D (Table S7).

The CH_4 adsorption energy on Ni–Si@2D strengthens with increasing work function, whereas the CO_2 adsorption energy exhibits a volcano-shaped trend (Fig. S3b). The Ni atom in Ni–Si@2D was identified as the primary activation site for CH_4 dissociation (Fig. 2 and Table S9), with Ni–Si@h-BN exhibiting the lowest barrier (0.50 eV), outperforming Ni–Si@GR, Ni–Si@P, and Ni–SiN $_4$ @GR. The Bader charge analysis of the C–C coupling step (Table S10) reveals that electrons transfer

from the CH₃-TM bond to CO₂, facilitating C-C bond formation. Ni-Si@h-BN exhibits a barrier of 0.71 eV for C-C coupling, which is comparable to other Ni-Si@2D systems and lower than the reported E-R pathway catalysts. 19 During acetic acid formation and desorption, most hydrogenation reactions proceed easily on Ni-Si@2D. For Ni-Si@2D catalysts at 500 K, the energy span is smallest on h-BN (1.26 eV), indicating its superior activity. While TS2 (C-C coupling) is the TDTS across all systems, the TDI differs: it is CH₃COO* + H* on Ni-Si@h-BN whereas it is adsorbed CH4* on the others. Together with fast CH₄ dissociation, facile C-C coupling, and favourable hydrogenation, Ni-Si@h-BN exhibits markedly enhanced activity compared with other reported catalysts (Table S11). By-product formation during acetic acid synthesis on Ni-Si@h-BN was also evaluated. Energetic span analysis shows that the C–C coupling pathway to CH_3COO^* ($\delta E = 0.71$ eV) is much more favorable than CO2 hydrogenation routes via COOH or HCOO ($\delta E = 1.97$ and 0.81 eV), indicating that C-C coupling dominates over formic acid formation (Fig. S12).

To further understand temperature effects, the energetic span was analysed at different temperatures, and the corresponding TDTS and TDI are summarized in Table S12. Ni–Si@ h-BN exhibits the lowest δE across 300–900 K, reaching 1.23 eV at 600 K (Fig. S13). Based on the energetic span model, the TOFs for acetic acid formation (300–900 K, 1 bar)²³ were calculated (Fig. 3), showing consistently high TOFs for Ni–Si@h-BN, with a peak at 700 K (8.02 \times 10⁻² s⁻¹, log TOF: 2.90), after which the TOFs decrease with further temperature increase. These results highlight Ni–Si@h-BN as an efficient catalyst for CH₄ and CO₂ conversion under moderate conditions while minimizing coke formation.²⁴

Understanding the relationship between catalytic performance and electronic properties is crucial for designing new

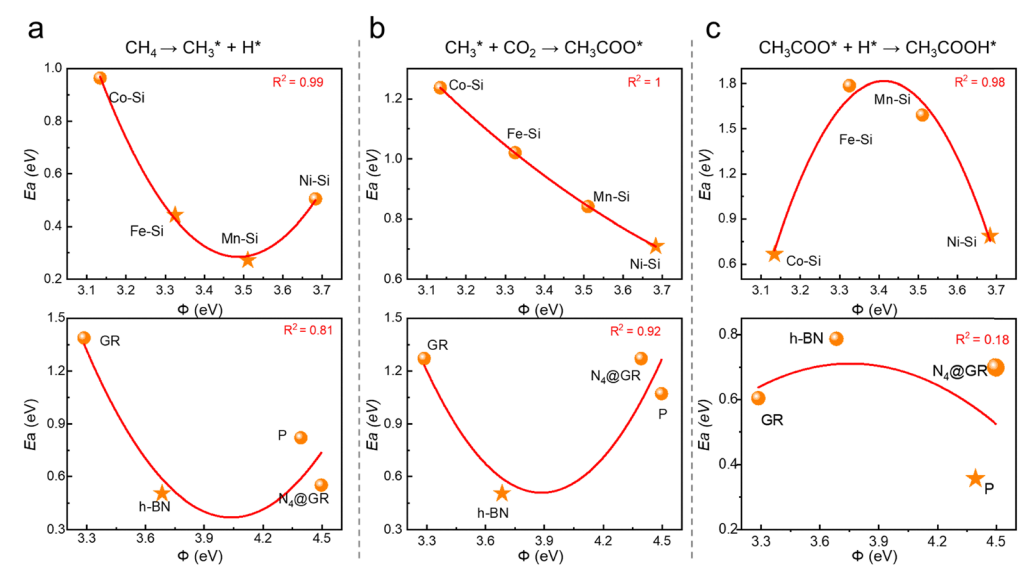


Fig. 4 Relationship between work function (ϕ) and energy barriers (E_a) for acetic acid synthesis from CH₄ and CO₂ on TM-Si@2D at 500 K: (a) CH₄ dissociation; (b) C-C coupling; (c) acetic acid formation. Upper panel: The 2D material is h-BN, lower panel: the transition metal is Ni-Si on different 2D materials.

Communication ChemComm

catalysts for efficient CH₄-CO₂ coupling toward acetic acid. CH₄ dehydrogenation on TM-Si@2D exhibits a volcano dependence on work function (Fig. 4a), with the lowest barriers with moderate values (3.3-4.0 eV) due to optimal polarization of the C-H bond. For C-C coupling (Fig. 4b), most TM-Si@2D follows a volcano-like behaviour, whereas TM-Si@h-BN shows a nearly linear decrease in barrier with increasing work function, benefiting from π back-donation that enhances CO2 adsorption and facilitates CH3* activation. In contrast, CH₃COO hydrogenation follows an inverse volcano relationship to the work function (Fig. 4c), showing reduced barriers at both low and high work function values. Bader charge analysis (Fig. S14) further confirms that higher TM electron density generally is attributed to reduced barriers throughout the entire reaction process. Ni-Si@h-BN, characterized by an electronrich Ni site (Ni^{-2.16}) and a moderate work function (3.68 eV), exhibits the lowest barrier in the rate-determining step and thus maintains thermodynamic favourability across all three elementary steps. This results from its balanced electron donation to the substrate with optimal adsorption strength.

We elucidated the acetic acid synthesis mechanism from CO2 and CH4 and designed TM-Si@2D based on DFT calculations. Silicon incorporation enriches transition metals with electrons, generating electron-rich active sites that enhance the catalytic activity. Ni-Si@h-BN stands out among doped transition metal catalysts. Its moderate work function and high Ni electron density facilitate CH_4 activation, while the $TM_1^{\delta^-}$ $Si_1^{\delta^+}$ synergy enables C-C coupling through the E-R mechanism. The turnover frequency for CH4 and CO2 conversion to acetic acid reaches $8.02 \times 10^{-2} \text{ s}^{-1}$ at 700 K and 1 bar, demonstrating the reaction's feasibility under practical conditions. This advantageous electronic structure underpins its capability for efficient and selective acetic acid synthesis.

This study was supported by the National Natural Science Foundation of China (No. 22172083, 22462020), the 111 Project (D20033), Inner Mongolia Science and Technology Planning Programme (2025YFKL0002). We also acknowledge Inner Mongolia China HPC Technology Co. LTD and Kelvin2 from NI-HPC at Queen's University Belfast for its Super-Server for the DFT calculations.

Conflicts of interest

There are no conflicts to declare.

Data availability

The data supporting this article have been included as part of the supplementary information (SI). Supplementary information is available including computational details, adsorption energies and work function, binding energies, Bader charges, activation energies, reaction energies, the structures and key geometry parameters of the reaction states, by product

formation pathways, and energy spans calculated at different temperatures. See DOI: https://doi.org/10.1039/d5cc04864h.

Notes and references

- 1 (a) Y. Li, K. Zheng, Y. Shen, M. Huang, B. Liu, Y. Xu and X. Liu, J. Phys. Chem. C, 2023, 127, 5841-5854; (b) B.-S. Mu, Y. Zhang, M. Peng, Z. Tu, Z. Guo, S. Shen, Y. Xu, W. Liang, X. Wang, M. Wang, D. Ma and Z. Liu, Angew. Chem., Int. Ed., 2024, 63, e202407443.
- 2 X. Zan, S. Tao, C. Zhang, Y. Wu, Y. Liu and W. Huang, J. Energy Inst., 2024, 116, 101739.
- 3 Y. Fujiwara, Y. Taniguchi and K. Takaki, Stud. Surf. Sci. Catal., 1997, **107**, 275–278.
- 4 I. H. Hristov and T. Ziegler, Organometallics, 2003, 22, 3513-3525.
- 5 S. Chempath and A. T. Bell, J. Am. Chem. Soc., 2006, 128, 4650-4657.
- 6 (a) Z. Riguang and B. W. Wei H, Chin. J. Catal., 2008, 29, 913; (b) Y. Liu, N. Cui, P. Jia and W. Huang, Catalysts, 2020, 10, 131; (c) N. Shahzad and B. Khan, J. Mol. Graphics Modell., 2021, 105, 107896,
- 7 A. M. Rabie, M. A. Betiha and S. E. Park, Appl. Catal., B, 2017, 215,
- 8 R. Shavi, J. Ko, A. Cho and J. W. Han, Appl. Catal., B, 2018, 229, 237-248.
- 9 (a) J. Chen, W. Xu and H. Zhang, ACS Appl. Nano Mater., 2024, 7, 11285-11294; (b) N. Liu, N. Lu and K. Zhao, Chem. Eng. J., 2024, 487, 150690.
- 10 C. Tu, X. Nie and J. G. Chen, ACS Catal., 2021, 11, 3472-3482.
- 11 X. Nie, X. Ren and C. Tu, Chem. Commun., 2020, 56, 3983-3986.
- 12 (a) C. Liu, X. Li and Y. Wang, ChemCatChem, 2016, 8, 421-433.; (b) B. Hu, H. Yang and Y. Luo, J. Catal., 2019, 369, 331-343.; (c) H. Wu, A. Singh-Morgan and K. Qi, ACS Catal., 2023, 13, 5375-5396; (d) L. Zhu, Y. Lin and K. Liu, Chin. J. Catal., 2021, 42, 1500-1508
- 13 (a) Y. Wang, G. Wu, M. Yang and J. Wang, J. Phys. Chem. C, 2013, 117, 8767-8773; (b) D. Kiani and I. E. Wachs, ACS Catal., 2024, 14, 16770-16784.
- 14 M. H. Mahyuddin, S. Tanaka and Y. Shiota, Bull. Chem. Soc. Jpn., 2020, 93, 345-354.
- 15 (a) D. Kiani and I. E. Wachs, ACS Catal., 2024, 14, 16770-16784; (b) J. Wang, Q. Song, Y. Shang, Y. Liu and J. Zhao, Nanomaterials, 2023, 15, 1111.
- 16 (a) R. Benrabaa, A. Löfberg and A. Rubbens, Catal. Today, 2013, 203, 188-195; (b) J. Niu, J. Ran and D. Chen, Appl. Surf. Sci., 2020, 513, 145840; (c) J. Li, E. Croiset and L. Ricardez-Sandoval, Appl. Surf. Sci., 2014, 311, 435-442.
- 17 (a) Y. Wang, L. Yao and Y. Wang, ACS Catal., 2018, 8, 6495-6506; (b) L. Li, Y. Wang and Q. Zhao, Catalysts, 2021, 11, 1–14.
- 18 (a) J. Feng, H. Gao and L. Zheng, Nat. Commun., 2020, 11, 1-8; (b) J. Yuan, W. Zhang and X. Li, Chem. Commun., 2018, 54, 2284-2287; (c) K. Homlamai, T. Maihom and S. Choomwattana, Appl. Surf. Sci., 2020, 499, 143928.
- 19 (a) P. Zhang, X. Yang and X. Hou, Catal. Sci. Technol., 2019, 9, 6297-6307; (b) R. Li, J. Wu and X. Zhao, Chem. Eng. J., 2024, 490, 151528.
- 20 (a) J. M. Zamalloa-Serrano, J. I. Mendieta-Moreno and J. M. Gómez-Fernández, Carbon, 2024, 229, 119544; (b) Y. Cheng and J. Zhou, iScience, 2024, 27, 108788.
- 21 L. Cui, K. Shi and M. Zhang, Fuel, 2023, 340, 127541.
- 22 (a) S. Kozuch and S. Shaik, Acc. Chem. Res., 2011, 44, 101-110; (b) J. Chen, Y. Chen, P. Li, Z. Wen and S. Chen, ACS Catal., 2018, 8,
- 23 (a) Y. Zhao, H. Wang, J. Han, X. Zhu, D. Mei and Q. Ge, ACS Catal., 2019, 9, 3187-3197; (b) A. M. Rabie, M. M. Hassan, E. A. El-Sharkawy and A. E. Awadallah, Appl. Catal., B, 2017, 215, 50-59; (c) M. G. Sibi, S. Chandran, R. C. Devarajan and N. R. Shiju, ACS Catal., 2021, 11, 8382-8398.
- 24 (a) L. He, M. Li, W.-C. Li, W. Xu, Y. Wang, Y.-B. Wang, W. Shen and A.-H. Lu, ACS Catal., 2021, 11, 12409-12416; (b) J. W. Han, C. Kim, J. S. Park and H. Lee, ChemSusChem, 2014, 7, 451-456.